TOPOLOGY OPTIMIZATION OF AN ADDITIVELY MANUFACTURED BEAM

Brian Torries[1], Saber DorMohammadi[2], Frank Abdi[2], Scott Thompson[1], Nima Shamsaei[1,*]

[1]*Laboratory for Fatigue & Additive Manufacturing Excellence, Department of Mechanical Engineering, Auburn University, Auburn, AL 36849*

[2] *AlphaSTAR Corp., 5150 East Pacific Coast Highway, Suite 650, Long Beach, CA 90804*

*Corresponding author: shamsaei@auburn.edu

Abstract

This study investigates the application of topological optimization in conjunction with additive manufacturing (AM) process simulation for fabricating parts that meet strict quality and performance requirements while also minimizing printed geometry. Integrated Computational Materials Engineering (ICME) and GENOA 3D commercial software were used to simulate specimen fabrication and, along with commercial design optimization tools, create an optimized beam topology for simple loading conditions. Constraints were set in order to support any over-hanging material with an appropriate inclination angle. These specimens were fabricated from Ti-6Al-4V using an EOS M290 direct metal laser sintering (DMLS) system with default parameters, as well as 95%, 90%, and 88% of default laser power in order to reduce the porosity in the over-heated areas. Parts were subjected to X-ray CT scanning to quantify part porosity. It was determined that the process used allowed for the fabrication of specimens with optimized topology and minimal defects.

Keywords: Additive manufacturing; Topology Optimization; Defects distribution; Porosity; ICME
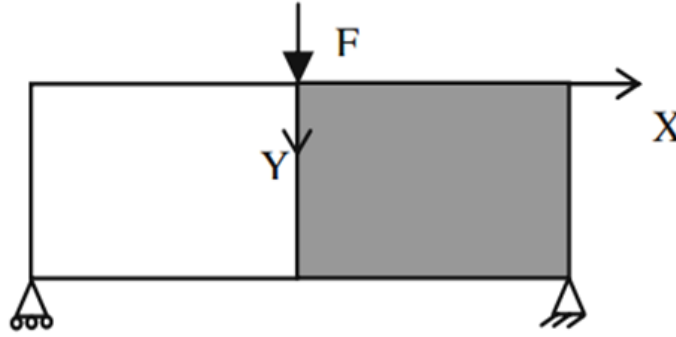
Introduction

Additive manufacturing (AM) is a promising avenue for manufacturing geometries that are difficult or impossible to produce through normal means, such as internal channels and high resolution features [1, 2], variable thickness walls, and parts already in an assembly [2]. However, while these new capabilities open up new design spaces, AM also comes with its own unique limitations. For example, there are support design considerations such as the minimum inclination angles that can be built without requiring supports, dimensional accuracy, and minimum wall thickness [2]. Additionally, the component size is limited by the volume of the AM machine [2]. The limitations vary by process and even by machine. Additionally, while AM can be used as a cost saving measure to create otherwise impossible to fabricate parts and repair costly parts, the material used to produce and repair these parts can be costly[1, 3]; therefore, it is important to design parts that are optimized not only for the intended application, but also to save material. The goal of topology optimization is to find the best distribution of limited material to minimize compliance subject to constraints affecting the design; therefore, pairing topology optimization with AM allows for the exploration of innovative geometries that would be difficult or impossible to produce through traditional manufacturing techniques while minimizing material, and therefore monetary, cost.

While many geometries can be created with AM, the time variant heat transfer and cooling rates of AM processes can result in non-uniform microstructures vastly different from those found in the wrought material [4-10]. Due to this, the mechanical properties of the mechanical part can vary across the geometry, leading to portions of the AM material not meeting application requirements. This has been seen in the investigation of AM AISI P20 steel and the effect of inter-layer time interval on AM specimens by Costa et al. [11]. The more uniform temperature profiles were found to lead to more uniform microstructure and hardness [11]. In order to produce a part with more homogenous mechanical properties, the deposition can be simulated and the geometry can be monitored for regions of under-heating and overheating. Once these regions have been identified, the build parameters in those areas can then be adjusted in order to produce a more uniform temperature profile, resulting in more uniform microstructure and mechanical response.
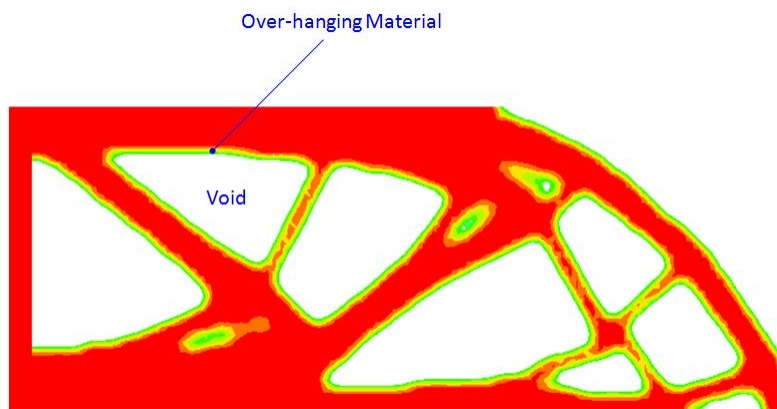
The goal of this study was to develop a process that integrated topological optimization with AM process simulation in order to produce as-built AM parts that would meet the quality and performance requirements for the specified application, without additional machining or modification. In order to accomplish this, a simply supported beam geometry was chosen as a test case. An off-the-shelf topological topology optimization tool was used in order to remove overhangs, eliminate the need for additional supports, and make the designed geometry able to be printed by Laser Powder Bed Fusion (L-PBF). In order to simulate the AM process and detect critical areas, the GENOA 3D printing software was applied to the geometry. Once the critical areas were identified, a sensitivity analysis was run on the laser power used in the simulation to find nodes in these areas containing over- and under-heating. Using these results, four additive specimens were manufactured: one with baseline parameters, and one each with 95%, 90%, and 88% baseline laser power. X-ray tomography was then conducted in order to determine the porosity of the fabricated specimens. It was determined that this process allowed for the fabrication of specimens with optimized topology and minimal defects.

Experimental Procedure

In order to test the simulation, a geometry had to be selected. For this study, a simply supported beam, shown in Figure 1, was settled on. Due to the symmetry of the part, only half of the beam, shown in Figure 1 as the grey portion, was optimized and printed. The off-the-shelf optimization software, OptiStruct, by Altair Engineering was applied to this half-beam geometry. Optistruct is based on the Solid Isotropic Microstrucutre with Penalization (SIMP) topology optimization theory, developed by Bedsøe in 1989 [12]. The SIMP method generates a continuous density voxel field associated with each element of the design domain. Based on a threshold value, ρ_t, this continuous field is converted into a voxel array, and smooth interior and exterior surfaces are generated by the software. Any elements found to have a density of less than 0.5 were removed and the smoothed, producing the final geometry used in this study, shown in Figure 2.
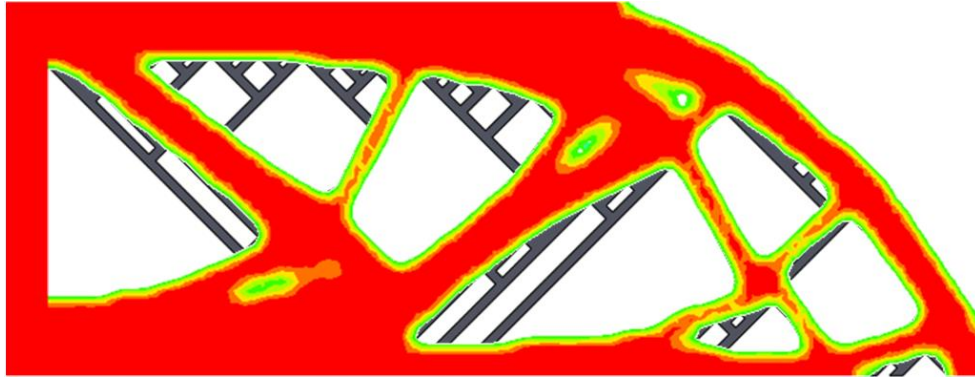
Figure 1. Simple beam geometry to be optimized

Figure 2. Optimized specimen geometry

Although Optistruct optimized the geometry for load bearing capacity and mass, it was necessary to refine this geometry in order to fit within the manufacturing geometric constraints of L-PBF. This refinement considered the minimum feature size (minimum section size, t_{min}), minimum manufacturable inclination angle (minimum inclination with respect to the horizontal at which an unsupported structure can be manufactured, α), and accommodation of heat transfer as critical design constraints. While the machine used to print the optimized geometry could accommodate an angle of inclination of 30° for Ti-6Al-4V, the more conservative angle of 45° was used to divide the geometric features into two categories: the robust zone, where the angle of inclination was greater than or equal to 45°, and the failed zone, where the angle of inclination was below 45°. In order to ensure successful builds, dedicated support material was put in place at all of the failed zone surfaces in order to enable AM [13]. There are drawbacks to such heavy-handed measures, such as increases in part weight, manufacturing time, and cost. Therefore, a novel approach was implemented in order to determine which surfaces lied outside of the robust zone and modify the identified geometry in order to allow for support-free manufacturing. Using a custom algorithm developed to accommodate infeasible domains with internal and external boundaries, the modified geometry is iteratively defined with a support inclination angle of 45°

and a minimum offset thickness of 0.5 mm until the geometry can be fabricated with a minimum of support material. The final geometry obtained through this method is shown in Figure 3.

Figure 3. Final Geometry edited for L-PBF fabrication. The red portion represents the original optimized geometry, while the grey represents the added support to allow for the geometry to be manufactured.
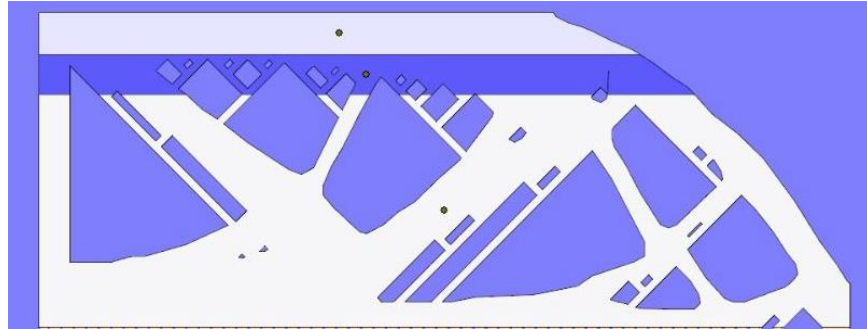
After the optimized geometry was finalized, a parametric study was performed with GENOA-3D in order to determine overheating and under-heating caused by the laser during the deposition process. Overheating and under-heating result in uneven temperature profiles, leading to less homogenous microstructure and mechanical properties. Using comparative values from the thermal field, the temperature at each node, T_{node}, is compared to T_{minT} and T_{maxT}. Once the area of interest, which contained the most over- and under-heated nodes, was determined through simulation, the simulation was iterated with different laser powers in an effort to find a laser power that would produce a more uniform thermal field. The laser powers investigated in this study were 280 W, 266W, 252 W, and 246 W, or baseline, 95%, 90%, and 88% laser power, respectively. It was found that the 95% laser power provided the best mix of under and overheated nodes in the areas predicted to have overheating by GENOA3D; the results of these simulations are presented in Table 1.

Table 1. Under- and Over-Heating predicted at different laser power.

Laser Power	Overheat	Under-heat
Baseline	308	0
95% Laser Power	283	1
90% Laser Power	221	7
88% Laser Power	208	8

The optimized beam geometry was fabricated using the aforementioned laser powers, a travel speed of 1200 mm/s, and a hatch spacing of 0.14 mm. A layer thickness of 30 microns was chosen, with hatching orientation rotating 67° between each layer for all specimens. In order to accomplish the altered print parameters at the area of interest, the optimized geometry was sliced into three

separate .stl models, and stacked on top of each other, as shown in Figure 4. Baseline parameters were used in the white and grey areas, while the blue portion utilized the altered laser power. Specimens were oriented to be 45° with respect to the vertical in order to allow for point contact between the recoater blade and the specimen rather than face contact, and utilized 3 mm support structures. Additionally, the curved edge of the specimen faced the recoater blade, in order for the feature to 'lean' with the build path rather than into the build path, reducing stress input from the recoater to the specimen during fabrication.
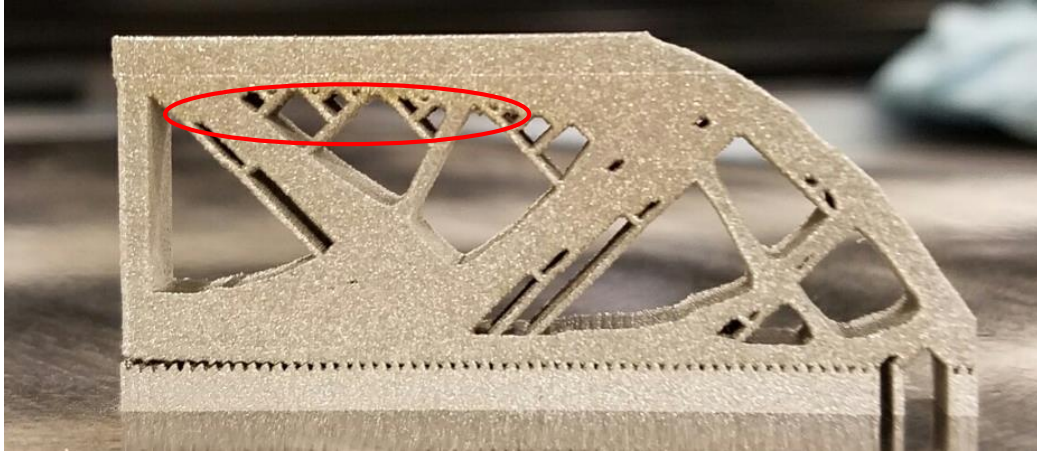

Figure 4. Sliced geometry used to alter printing parameters from baseline (white and grey areas) to lower laser power (blue area).

After the optimized geometry specimens were fabricated, x-ray tomography was conducted on the region of interest predicted to contain overheating for all of the specimens. All of the specimens were scanned in a single operation with a scan resolution of 16 μm.
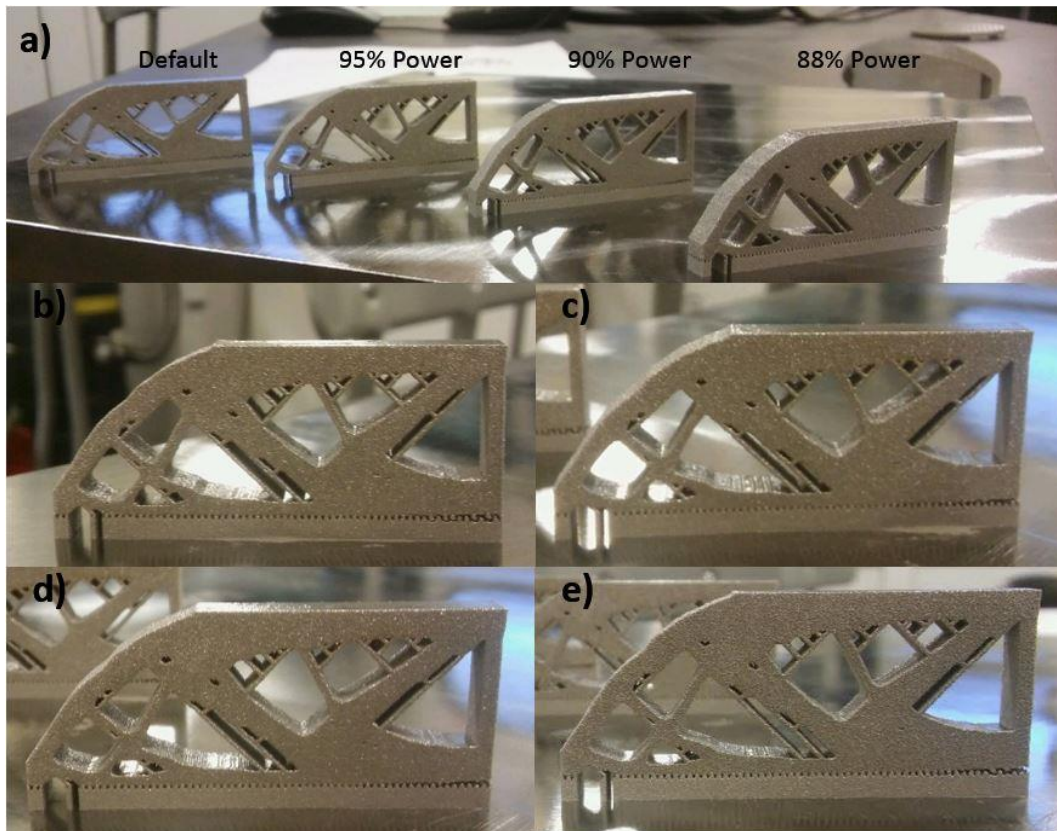
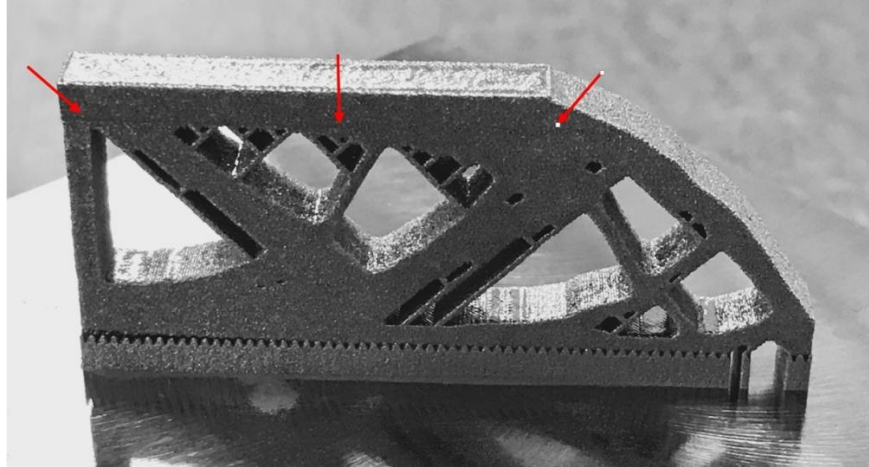## Results and Discussion

Printed Geometry
Figure 5 shows the results of printing a single optimized build geometry using the baseline parameters, while Figure 6 shows the results of printing the baseline, 95%, 90%, and 88% laser power specimens in the same build operation. The slight ridge, or "witness line" seen near the top of the specimen was caused by the machine running out of powder with approximately 100 layers of the build left. The specimen was allowed to cool in order to add more powder and finish the build; this lead to a larger temperature differential when the build resumed as compared to if the build had continued unhindered, resulting in the ridge. Note that overheating occurred in the predicted areas (marked by a red circle) on the single built baseline parameter specimen; this was absent in the specimens that utilized lower laser powers (Figure 6). The specimens that utilized lower laser power during fabrication exhibited a slight ridge where the altered parameters ended and the default parameters started, similar the witness line in Figure 5; this is shown in Figure 7, denoted by the red arrows.

Figure 5. Optimized geometry built by itself in a single build operation. Overheating (red circle) occurred in the predicted area.
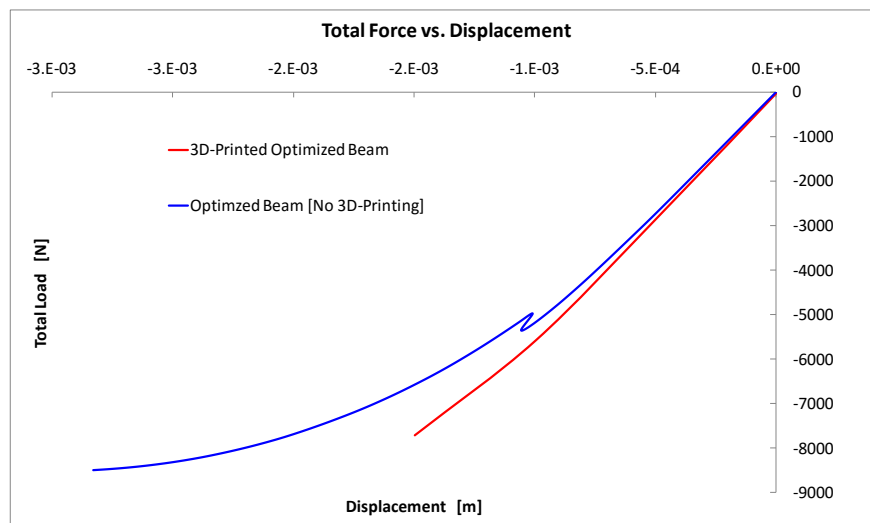

Figure 6. Optimized build geometry (a) overview and detail of specimens built with the (b) baseline, (c) 95% power, (d) 90% power, and (e) 88% power parameters.
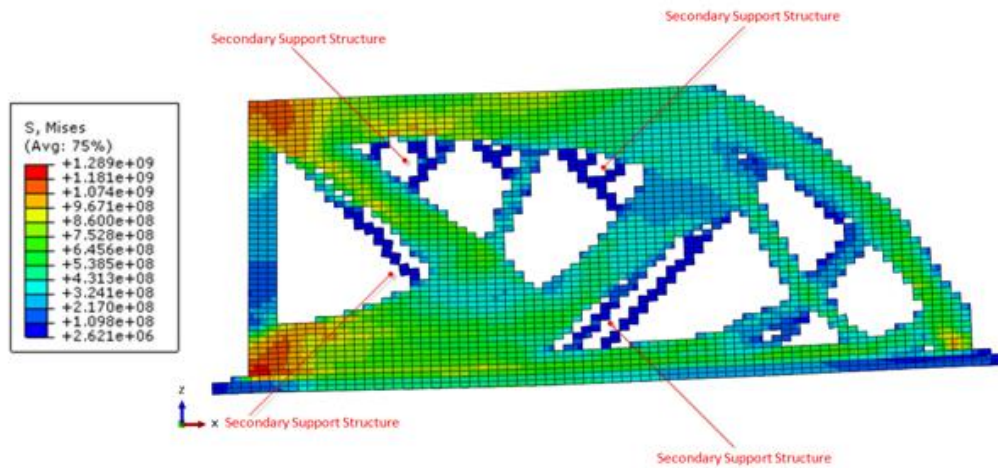
Figure 7. Slight ridge (marked by red arrows) exhibited by the specimen fabricated with 88% laser power in the area of interest.

Simulation Results

In order to determine if the optimized geometry met the stress criteria, a finite element analysis of the optimized beam geometry as-designed and as-printed under identical loading was performed, the results of which are shown in Figure 8. Note that for loads of up to 3,000 N the as-designed and as-printed geometries performed nearly identically, and for loads of up to approximately 5,250 N the performance was very close. At higher loads the behaviors depart dramatically, with the as-printed geometry not showing the spike in deformation behavior and overall exhibiting less deformation due to the applied force. It is interesting to note that the secondary supports added during the optimization process (grey supports in Figure 3) experienced negligible stresses as compared to the primary structure produced by the initial analysis, as shown in Figure 9. This supports the assertion that the initial geometry optimization was satisfactory, and that the added refinements only serve to allow for L-PBF fabrication of the specimen.
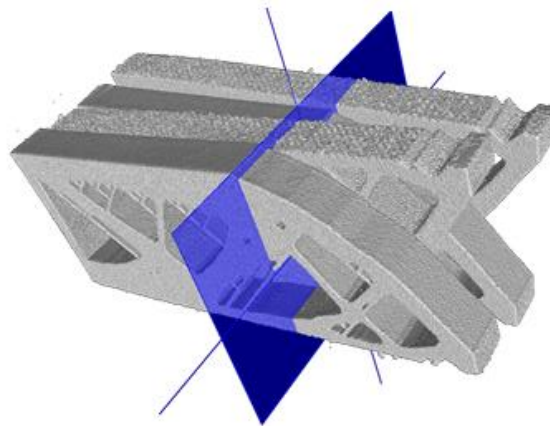

Figure 8. Simulated deformation upon displacement-control service loading for full beam, optimized beam, and 3D printed optimized beam geometry.

Figure 9. Finite element analysis showing stress concentrations in AM optimized beam geometry.

X-Ray Evaluation

After the specimens were removed from the build plate, the specimens were all investigated via x-ray tomography in order to quantify the porosity and surface roughness of the specimens. The results of the void and surface roughness calculations conducted at the midsection of the specimens on a plane perpendicular to the regions with altered parameters, denoted in Figure 10 by the blue plane, are given in Table 2. As the laser power decreased, the surface roughness increased. Additionally, while the 95% laser power specimen was predicted to have the optimal mix of under-heated and overheated nodes, it, along with the 90% laser power specimen, exhibited the highest void content of the specimens. The baseline specimen exhibited the least amount of void content. The 88% laser power specimen exhibited the highest surface roughness and exhibited a void content similar to the baseline specimen. It is important to note that this plane includes a cross section of the entire sample, not just the area with the adjusted build parameters; the differences in porosity could be the result of variation in the samples inherent to the additive process.

Figure 10. X-ray tomography of baseline, 95%, 90%, and 88% laser power samples. The plane the void and surface roughness measurements were taken at is shown in blue.

Table 2. X-ray tomography results.

Laser Power	Void Content	Surface Roughness
Baseline	2.5%	15.1
95% Laser Power	5.9%	20.7
90% Laser Power	5.9%	20.7
88% Laser Power	3.1%	24.3

Conclusions

In this project, a design tool was developed by integrating commercial topology optimization software (OptiStruct) and GENOA3D. The framework was utilized in topology optimization of simply-supported beam to be fabricated with AM without support structure. Process parameters were developed using GENOA3D to fabricate part with minimum defects in overhanging regions caused by under- and overheating. It was found that the framework design provides topology which can be fabricated without any additional manufacturing consideration. The specimens fabricated following software suggested process parameters were evaluated using X-ray CT and compared with baseline specimen. It was shown that software results improved the quality of the build. The following conclusions can be drawn from this study:

1. Integrating a commercial topology optimization software (OptiStruct) with GENOA3D produced a geometry that was not only optimized for a specific loading scenario, but also able to be manufactured by an additive manufacturing machine.
2. As the laser power increased in specimen production, the surface roughness of the specimen decreased.
3. The simulation could accurately predict areas of overheating and under-heating, as evidenced by the overheating in the singly manufactured specimen.

Future plans include further investigation of the x-ray data, including in-plane with the altered parameter regions, in order to determine if the void content found in the investigated plane is representative of the entire specimen, or if it is constrained to the areas where overheating was predicted. More complex geometries and a wider range of fabrication parameters will also be investigated, with microstructural investigations performed The results of this study show that not only are integrated topology optimization and structural modeling, such as the GENOA3D with integrated OptiStruct, a convenient tool to optimize build geometry in such a way as to allow for additively manufactured, but these tools can also aid in the selection and refinement of build parameters, allowing for less design iterations.

Acknowledgments

References

[1] Frazier, W.E, "Metal Additive Manufacturing: A Review," *Journal of Materials Engineering and Performance*, Vol. 23, No. 6, 2014, pp. 1917-1928.

[2] Atzeni, E., Salmi, A., "Economics of Additive Manufacturing for End-usable Metal Parts," *The International Journal of Advanced Manufacturing Technology*, Vol. 62, No 9-12, 2012, pp. 1147-1155.

[3] Sterling, A.J, Torries, B., Shamsaei, N., Thompson, S.M., Seely, D.W., "Fatigue Behavior and Failure Mechanisms of Direct Laser Deposited Ti-6Al-4V," *Materials Science and Engineering A*, Vol. 655, 2016, pp. 100 – 112.

[4] Sterling, A.J., Shamsaei, N., Torries, B., Thompson, S. M., "Fatigue Behaviour of Additively Manufactured Ti-6Al-4V," International Conference on Fatigue Design, Senlis, France, 2015.

[5] Brandl, E., Leyens, C., Palm, F. "Mechanical Properties of Additive Manufactured Ti-6Al-4V using Wire and Powder Based Processes," Trends in Aerospace Manufacturing 2009 International Conference, TRAM09, IOP Conference Series: Materials Science and Engineering 26, 2011.

[6] Wu, Xinhua, et al, "Microstructures of Laser-deposited Ti-6Al-4V," Materials and Design, Vol. 25, No. 2, 2014, pp. 137-144.

[7] Mutombo, K, 2013, "Metallurgical Evaluation of Laser Additive Manufactured Ti6Al4V Components" Rapid Product Development Association of South Africa (RAPDASA) Conference, SanParks Golden Gate Hotel, South Africa.

[8] Selcuk, C., "Laser Metal Deposition for Powder Metallurgy Parts," Powder Metallurgy, Vol. 54, Issue 2, 2011, pp. 94-99.

[9] Shamsaei, N., Yadollahi, A., Bian, L., Thompson, S. M., "An Overview of Direct Laser Deposition for Additive Manufacturing; Part II: Mechanical Behavior, Process Parameter Optimization and Control," Additive Manufacturing, Vol. 8, 2015, pp. 12-35.

[10] Gammon, L. M., Briggs, R. D., Packard, J. M., Batson, K. W., Boyer, R., Domby, C. W., "Metallography and Microstructures of Titanium and Its Alloys," ASM Handbook, Vol. 9, 2004, pp. 899-917.

[11] Costa, L., Vilar, R., Reti, T., Deus, A. M., "Rapid Tooling by Laser Powder Deposition: Process Simulation Using Finite Element Analysis," Acta Materialia, Vol. 53, Issue 14, 2005, pp. 3987 – 3999.

[12] Bedsøe, M.P., "Optimal Shape Design as a Material Distribution Problem," *Structural optimization*, Vol. 1, No. 4, 1989, pp. 193-202.

[13] Leary, M., Merli, L., Torti, F., Mazur, M., Brandt, M., "Optimal Topology for Additive Manufacture: A Method for Enabling Additive Manufacture of Support-free Optimal Structures," *Materials and Design*, Vol. 63, 2014, pp. 678-690.